

Materials subjected to fast neutron irradiation/Matériaux soumis à irradiation par neutrons rapides

Radiation effects in concentrated alloys and compounds: equilibrium and kinetics of driven systems

Georges Martin^a, Pascal Bellon^{b,*}

^a CEA-Siège, Cabinet du haut commissaire, 91191 Gif-sur-Yvette cedex, France

^b Department of Materials Science and Engineering, University of Illinois at Urbana-Champaign, Urbana, IL 61801, USA

Available online 3 April 2008

Abstract

What organization of condensed matter does resist irradiation, as a function of irradiation conditions? How to characterize the latter? We survey the advances in the field during the past three decades, when irradiation effects reduce to nuclear collisions. While in simple cases (structure defined by a scalar order parameter) one may define a stochastic potential, which yields the stationary states of the compounds under irradiation and their respective stability, in more general cases, we are left with brute force atomistic simulations to explore materials' behaviour as a function of irradiation conditions. Special attention is given to the kinetics of concentration fields under irradiation, a question with several practical implications. We conclude that irradiation conditions are best defined by three parameters: the cascade features (number of displacements and replacements, length of replacement sequences, . . .), the frequency of cascade occurrence, and the cumulated dose. We suggest cascade features be named '(elementary) dose' and the cascade occurrence frequency 'dose rate'. **To cite this article: G. Martin, P. Bellon, C. R. Physique 9 (2008).**

© 2007 Académie des sciences. Published by Elsevier Masson SAS. All rights reserved.

Résumé

Effets d'irradiation dans des alliages concentrés et des matériaux complexes : équilibre et cinétique des systèmes. Quelle organisation de la matière résiste à l'irradiation, suivant les conditions d'irradiation ? Comment caractériser ces dernières ? Nous résumons les progrès réalisés au cours des trois dernières décennies, dans la limite où les effets d'irradiation se réduisent aux collisions nucléaires. Dans les cas simples (structure définie par un paramètre d'ordre scalaire) on peut construire un potentiel stochastique qui fournit les états stationnaires et leur stabilité respective ; dans les cas plus généraux, on est réduit à explorer, par des simulations numériques, le comportement du matériau en fonction des conditions d'irradiation. On discute la cinétique des champs de concentration sous irradiation, une question aux multiples conséquences pratiques. Il ressort que les conditions d'irradiation sont définies par trois paramètres : les caractéristiques de la cascade (le nombre de déplacements et de remplacements, longueur des chaînes de remplacements, . . .), la fréquence d'apparition des cascades et la dose cumulée. Une clarification de vocabulaire consisterait à dénommer la cascade « dose (élémentaire) », leur fréquence d'apparition étant le « débit de dose ». **Pour citer cet article : G. Martin, P. Bellon, C. R. Physique 9 (2008).**

© 2007 Académie des sciences. Published by Elsevier Masson SAS. All rights reserved.

Keywords: Radiation damage; Complex materials

Mots-clés : Endommagement par irradiation ; Matériaux complexes

* Corresponding author.

E-mail address: bellon@uiuc.edu (P. Bellon).

1. Introduction

Irradiation may trigger electronic excitations, nuclear reactions and nuclear collisions at a frequency that is determined by the dose rate. Under such circumstances, materials experience a permanent evolution: electronic excitations modify the chemical bonding in insulators, nuclear reactions alter the chemical composition of any material, nuclear collisions trigger atomic mixing and produce point defects (isolated or as small clusters). The long term evolution of the latter modifies the microstructure in the broad sense, i.e. the dislocation density, the grain size, the precipitate size and composition, . . . These evolutions may be modeled with several techniques, the efficiency of which has been improving rapidly, during the past two decades. However, the question of the structural stability of a compound under irradiation is still a broadly open question. As examples we quote: is SiC a stable compound under appropriate irradiation conditions (stable e.g. with respect to the decomposition into Si and C, crystalline or amorphous)? What about the FeCr solid solutions, which are the basis of ferritic alloys: will the latter decompose into two distinct phases (Cr poor and Cr rich)? What about the stability of UO₂ (with respect to U₄O₉), the widely used fuel material as a function of composition and temperature? What about the various minerals studied as potential waste confinement materials? What about glasses?

Any compound under irradiation experiences a competition between ‘damaging’ and ‘healing’ processes. The higher the irradiation dose rate, the more frequent the damaging processes; the higher the temperature, the faster the healing processes (at least for diffusion controlled restoration). Therefore one guesses that the stability of one given form of a compound, with a given composition, depends at least on the temperature and *on the dose rate*; by ‘the form of a compound’ we mean e.g. uniform solid solution versus two-phase alloy, ordered versus disordered, ordered with one or another crystallographic structure, crystalline versus amorphous, etc. . . Moreover, since the healing kinetics is usually nonlinear, for a given dose rate, the resulting alloy structure will depend on whether the dose is delivered by rare large perturbations or frequent small perturbations. The former perturbations are, for instance, the displacement cascades produced by neutron or heavy ion irradiations, while the latter are found in the short replacement collisions that accompany the formation of a single Frenkel pair when the energy transferred to the primary knocked atom is close to the displacement threshold energy.

On top of the above underlying competition, whenever the crystalline structure is conserved, the agglomeration and elimination of point defects at defect sinks slowly alters the sink strength, and as a consequence, the mean point defect concentration, which controls the atomic mobility. Also, transmutations superimpose a slow drift of the composition.

Such a complexity should not prevent us from looking for methods to assess the stability of various compounds under irradiation. For a given composition and for a given sink strength, what is the stable form of the compound, as a function of the irradiation dose rate and irradiation temperature [1]?

2. Irradiation induced phase transformations, as observed experimentally

Most materials are prepared and used with a non-equilibrium structure, because solid-state diffusion is sluggish. As soon as neutron sources became available, it was recognized that irradiation might be used to enhance the rate of relaxation toward equilibrium: an historical example is the identification of the FeNi ordered phase after low temperature neutron irradiation, a phase that cannot be formed by thermal aging [2]. Such a transformation (from the random solid solution to an ordered compound) is *enhanced* by irradiation. The mechanism for the latter enhancement is that diffusion in the solid-state proceeds by exchanges of site between atoms and neighboring point defects: irradiation increases the defect concentration, hence increases the number density of those atoms which may change location per unit time.

Quite a distinct class of phenomena are *irradiation-induced transformations*, i.e. transformations that drive the system to a state that is distinct from its thermal equilibrium configuration. Self-irradiation induced amorphization of minerals has been known for a long time. However, for decades, this phenomenon has not been phrased in the words of a phase transformation, i.e. with a well-defined phase diagram: the identification of the irradiation conditions (temperature, dose rate, type of particle-matter interaction) that can stabilize the amorphous phase with respect to the crystalline one, in a given compound, is still a widely open question. The domain of stability of a given compound as a function of the irradiation conditions was determined experimentally, for the first time, in the mid 1970s. Fig. 1 shows, under 1 MeV electron irradiation, the dose rate and temperature conditions under which an *under-saturated* Ni(Si) solid solution separates into two phases (domain II), the solid solution and Ni₃Si precipitates. In domains I and III,

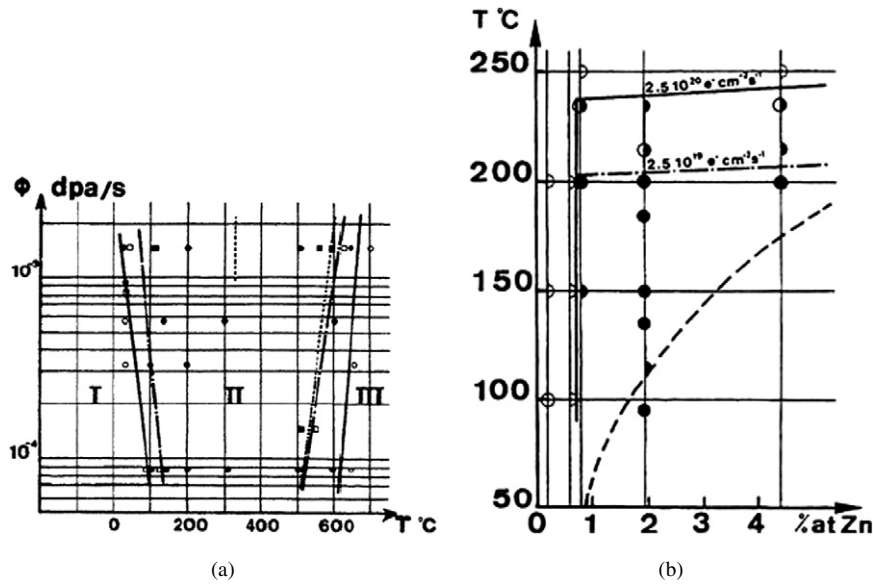


Fig. 1. (a) Dynamical equilibrium diagram for Ni(Si) under 1 MeV electron irradiation; in domain II Ni_3Si precipitates are formed, while in domains I and III, the solid solution is stable. The various lines correspond to various solute content; In thermal equilibrium, the solid solution would phase separate below $\approx 400^\circ\text{C}$. Irradiation induces precipitation above that temperature, i.e. in undersaturated solid solutions, and dissolves precipitates below 100°C . At a given irradiation intensity (10^{-3} displacements per atom per second – dpa s^{-1}), 150 keV Ni ion irradiations (vertical dotted line) are more efficient than 1 MeV electrons to dissolve precipitates (from Ref. [3a]). (b) Under intense 1 MeV electron irradiation, GP Zones form in Al(Zn) at temperatures (plain circles) well above the solvus temperature (dashed line). The maximum temperature for GPZ formation increases with the irradiation flux: from $\approx 200^\circ\text{C}$ under $2.5 \times 10^{19} \text{ e}^- \text{ cm}^{-2} \text{ s}^{-1}$ to $\approx 240^\circ\text{C}$ under $2.5 \times 10^{20} \text{ e}^- \text{ cm}^{-2} \text{ s}^{-1}$ (after Cauvin et al. [3b]).

Fig. 1. (a) Diagramme d'équilibre dynamique de phase pour Ni(Si) irradié aux électrons de 1 MeV ; dans le domaine II des précipités Ni_3Si se forment, tandis que dans les domaines I et III, la solution solide est stable. Les différentes lignes correspondent à différentes concentrations moyennes de soluté ; à l'équilibre thermique, la solution solide se décompose pour T inférieures à $\approx 400^\circ\text{C}$. L'irradiation induit une précipitation au-delà de cette température, c'est à dire dans des solutions solides sous-saturées, et dissous les précipités en-deçà de 100°C . Pour une intensité d'irradiation donnée (10^{-3} déplacements par atome par seconde – dpa s^{-1}), l'irradiation par des ions Ni de 150 keV (ligne verticale pointillée) est plus efficace que les électrons de 1 MeV pour dissoudre les précipités (d'après la Ref. [3a]). (b) Sous intense irradiation aux électrons de 1 MeV, des zones GP se forment dans Al(Zn) à des températures (cercles pleins) bien supérieures à la limite de solubilité (ligne pointillée). La température maximum pour la formation de zones GP croît avec le flux d'irradiation : de $\approx 200^\circ\text{C}$ pour $2,5 \times 10^{19} \text{ e}^- \text{ cm}^{-2} \text{ s}^{-1}$ à $\approx 240^\circ\text{C}$ pour $2,5 \times 10^{20} \text{ e}^- \text{ cm}^{-2} \text{ s}^{-1}$ (d'après Cauvin et al. [3b]).

the solid solution is stable under irradiation, as it is in the absence of irradiation. The various lines pertain to distinct overall compositions [3a]. The high temperature border of Domain II defines the conditions for *irradiation induced precipitation* in Ni(Si) solid solutions. Fig. 1 is a diagram for *dynamical equilibrium*, which we named '*dynamical equilibrium phase diagram*', by analogy with *thermal equilibrium phase diagrams*. *Dynamical* is to remember that the configurations, here, are stationary ones, where the destruction and restoring processes compensate one another, while energy is permanently pumped into the system, because of particle matter interaction. We refer to such systems as *driven alloys*.

Such dynamical equilibrium phase diagrams are scarce, and are certainly worth determining in more systems. Some examples are: the transition temperatures between various ordered structures in Ni_4Mo under irradiation by 1 MeV electrons, light and heavy ions [16], the solubility limit of Zn in Al under 1 MeV e^- irradiations (for detailed reviews, cf. [4,5]). Even though dynamical equilibrium phase diagrams were not determined extensively, many irradiation-induced transformations have been identified: several metallic under-saturated solid-solutions have been observed to undergo phase separation, sometimes with an unexpected structure for the second phase to appear (e.g. in W–Re); diamond C can be nucleated out of graphite with the onion like structure [6,7]; Si and other covalent materials are known to amorphize because of nuclear collisions, while electronic stopping accelerates recrystallization etc.

Also, unusual microstructures may be stabilized by irradiation. For instance, in a two-phase alloy, while under thermal conditions, larger precipitates grow at the expense of smaller ones (because of the capillary pressure), irradiation

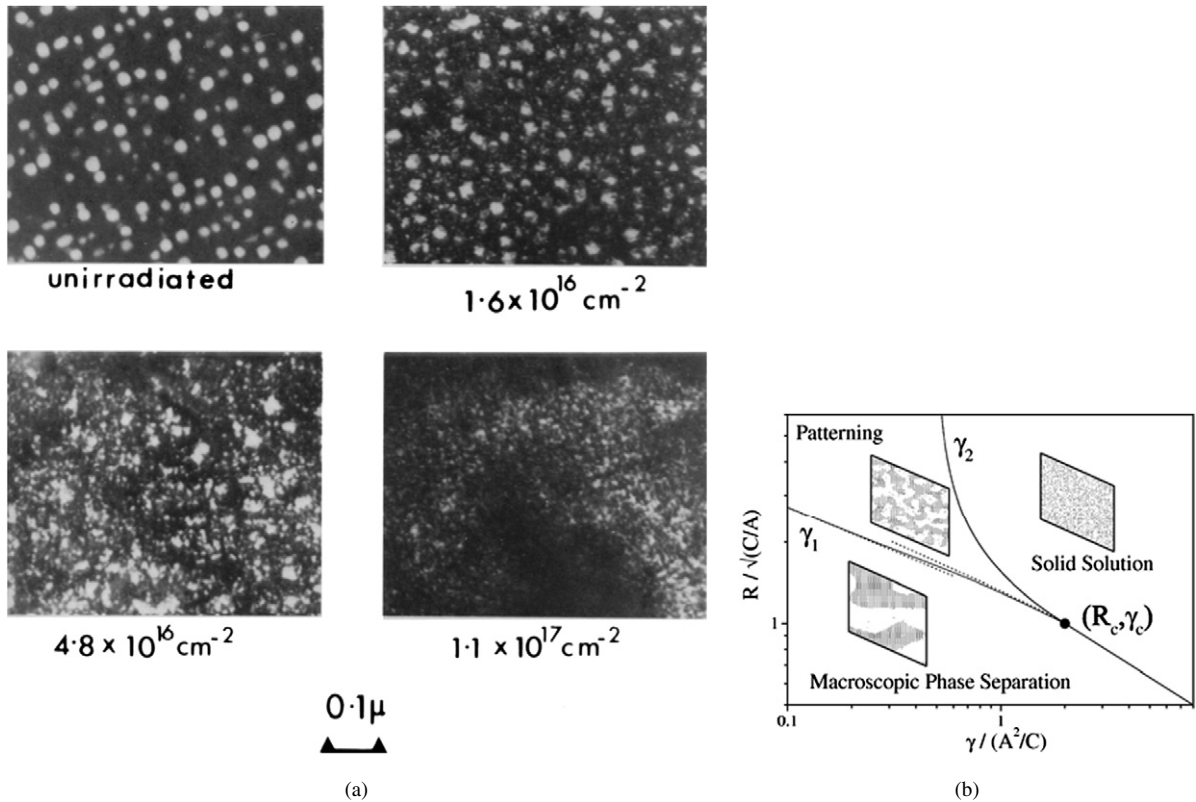


Fig. 2. (a) Dark field TEM imaging of $L1_2$ ordered Ni-rich precipitates in Ni-13.5at. %Al irradiated at 550 °C with 100 keV Ni ions; notice the refinement of the precipitate microstructure and the stabilization of nanoscale precipitates at large irradiation dose, in Ni ions cm^{-2} (from Ref. [11]). (b) Dynamical equilibrium phase diagram for an $A_{50}B_{50}$ alloy that undergoes phase separation at thermodynamic equilibrium. $\gamma = \Gamma_b/M$ is a dimensionless forcing intensity, and R is the average atomic relocation distance. The transition lines are calculated from an effective free energy. Insets are typical steady-state microstructures simulated by KMC simulations, observed here in a (111) plane (from Ref. [8]).

Fig. 2. (a) Images au MET en champ sombre des précipités ordonnés $L1_2$ dans un alliage Ni-13,5at. %Al irradié à 550 °C avec des ions Ni de 100 keV; on notera la réduction de la taille des précipités et leur stabilisation à une valeur stationnaire à forte dose (Ni ions cm^{-2}) (d'après Ref. [11]). (b) Diagramme d'équilibre dynamique de phase pour un alliage modèle $A_{50}B_{50}$ qui se décomposerait à l'équilibre thermodynamique. $\gamma = \Gamma_b/M$ est un paramètre réduit d'intensité d'irradiation, et R est la distance moyenne des remplacements. Les lignes de transitions sont calculées à partir d'une énergie libre effective. Les inserts sont des plans (111) de microstructures typiques simulées par Monte Carlo cinétiques (d'après Ref. [8]).

by certain particles may trigger a patterning of the microstructure at some length scale, which depends on the dose rate, the temperature, and the mean replacement distance of atoms in the collision cascades [8–10] (Fig. 2).

3. Theory and modeling of irradiation induced phase transformations

Irradiation-induced phase transformations are one example of transitions between (quasi-) stationary states of dynamical systems. The latter differ from thermal equilibrium systems, for which statistical and macroscopic thermodynamics offer an extremely powerful theoretical framework. In particular the stability of competing structures as a function of temperature, pressure and chemical composition can be assessed unambiguously. On the contrary, under irradiation, a compound is subjected to a steady flow of energy from the beam of incident particles to the thermostat (which fixes the temperature). While entropy can be defined, defining an effective free energy raises questions that are beyond the scope of this paper [12,13]. We rather summarize techniques, which helped rationalize various observations, with, sometimes, a predictive power. Comprehensive surveys are given in Refs. [4,5].

3.1. The weaknesses of macroscopic deterministic modeling

The competition between irradiation-induced damaging and thermal recovery is sometimes modeled in an intuitive manner. For instance, let us assume that the state of the material is characterized by some scalar S (degree of crystallinity, or long range order parameter, or residual solute content in a matrix, . . .). The time derivative \dot{S} of S can be written:

$$\dot{S} = \dot{S}^{\text{thermal}} - \dot{S}^{\text{irrad}} = -\partial L(S)/\partial S \tag{1}$$

The first term represents the recovery rate due to healing processes and the second term the damaging rate, which results from particle–matter interaction. $L(S)$ is the Lyapunov function of the problem. Stationary states are achieved whenever the healing rate equals the damaging rate, $\dot{S} = 0$, i.e. for the extrema of $L(S)$: a minimum corresponds to a locally stable stationary state, a maximum to an unstable state. Since the healing and damaging rates are in general non-linear functions of S , several stationary states are to be expected. As the latter rates depend (at least) on temperature (T) and irradiation intensity (Φ), one expects the stationary states to shift with these control parameters; also the local stability of one given state may change when changing (Φ, T): the shift may be smooth (as in second order transitions: ‘direct bifurcation’) or abrupt (as in first order transitions: ‘inverse bifurcation’).

The above approach has several shortcomings:

- (a) Guessing the analytical form of the recovery and damaging rates is risky. As an example, consider the growth of a precipitate (or a gas bubble) under irradiation; it is sometimes claimed (mostly in the fuel modeling community) that, under irradiation, a bubble grows by thermally activated jumps of gas atoms and decays because of ballistic ejection of gas atoms from the bubble surface into the matrix. Hence the thermal and ballistic growth rates have distinct dependence in the radius of the bubble: R for the thermal part, R^2 for the ballistic decay:

$$\partial n^{\text{therm}}/\partial t \propto 4\pi DR(c - c_{\text{eq}}); \quad \partial n^{\text{irrad}}/\partial t \propto -4\pi R^2 a \Gamma^{\text{bal}} c_p$$

where c_p, c and c_{eq} are respectively the volumetric gas concentration in the bubble, in the matrix, and the equilibrium value of the latter; a is the atom size. As a result of these assumptions and dependencies, a stable stationary radius is expected:

$$\bar{R} \propto (D/a\Gamma^{\text{bal}}) \frac{c - c_{\text{eq}}}{c_p};$$

as will be discussed in Section 3.3.1 below, this model incorrectly neglects ballistic jumps back to the bubble, and thus does not predict correctly the size saturation of precipitates.

- (b) Moreover, unlike the free energy for equilibrium states, the Lyapunov function does not give any information on the *respective stability* of two locally stable stationary states. The reason for this is that the deterministic description we start from has no noise term built in, unlike the thermal noise in equilibrium thermodynamics. For instance, Fig. 3 reveals two locally stable stationary states, $\bar{S} = 0, \bar{S} = \bar{S}_2$: which of these is the more stable one,

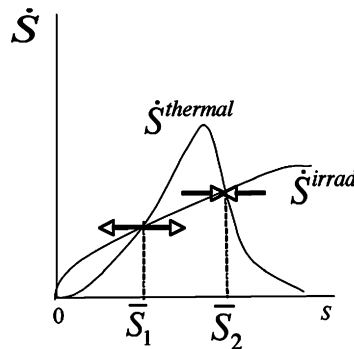


Fig. 3. A system with three stationary states: $\bar{S} = 0, \bar{S}_1, \bar{S}_2$, one of which, \bar{S}_1 , is unstable.
 Fig. 3. Une système à trois régimes stationnaires : $\bar{S} = 0, \bar{S}_1, \bar{S}_2$, dont l'un est instable, \bar{S}_1 .

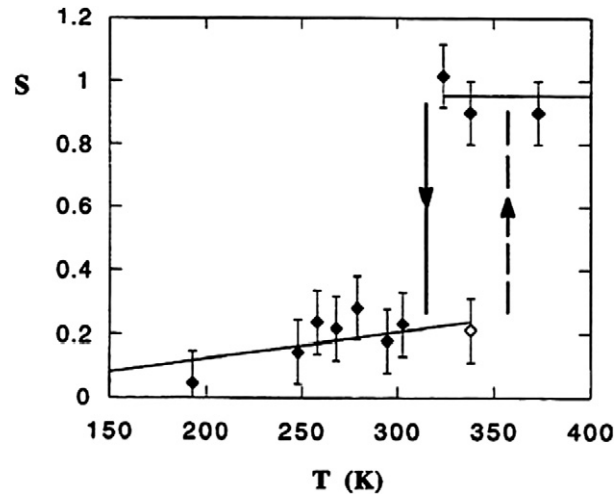


Fig. 4. Inverse bifurcation under irradiation: the stationary degree of long range order in the Fe–Al compound (B2 structure) under irradiation with $7 \times 10^{19} \text{ MeV e}^- \text{ cm}^{-2} \text{ s}^{-1}$, undergoes an abrupt decrease in the temperature range 320–360 K. The transition exhibits hysteresis (from Ref. [14]).

Fig. 4. Bifurcation inverse sous irradiation : le degré stationnaire d'ordre à grande distance dans le composé FeAl (de structure B2) irradié sous $7 \times 10^{19} \text{ MeV e}^- \text{ cm}^{-2} \text{ s}^{-1}$; ce degré d'ordre subit une chute abrupte dans l'intervalle de température 320–360 K. La transition possède une hystérésis (d'après la Ref. [14]).

depending on irradiation conditions? Can we observe coexisting stationary states, as in a first order transition?

Fig. 4 gives one example of a first order like transition, observed in the Fe–Al compound under intense 1 MeV electron irradiation (in a High Voltage Electron Microscope): the degree of long range order decreases abruptly at an irradiation temperature $\approx 350 \text{ K}$, with metastability between 320 and 360 K.

(c) Last but not least, while a Lyapunov function can always be defined for a scalar order parameter (as S , or R above), such is generally not the case for multi-dimensional order parameters.

The way to circumvent the above difficulties is to start from the dynamics of the material at the atomic scale.

3.2. Stochastic approach

We focus on the atomic configurations of the material (lattice gas model), and assume an instantaneous (at the time scale of the mean atomic jump period) thermalisation of the excitations created by the incident particles. The probability of a given microconfiguration, i , is governed by the master equation, where the transition probabilities $W_{i;j}$ are written as a sum of two contributions: that resulting from the coupling with the thermal bath (labeled 'th' for 'thermal'), and that resulting from particle-matter interaction (which we name 'ballistic', labeled 'bal'):

$$\partial_t P_i = \sum_{\{j\}} (-P_i W_{i;j} + P_j W_{j;i}); \quad W_{j;i} = W_{j;i}^{\text{th}} + W_{j;i}^{\text{bal}} \quad (2)$$

The stationary state corresponds to a divergence-less probability flux:

$$\sum_{\{j\}} \bar{J}_{ij} = 0 \quad \forall i; \quad J_{ij} = P_i W_{i;j} - P_j W_{j;i} \quad (3)$$

In the case of thermal equilibrium, the detailed balance argument imposes that the probability flux is equal to zero, i.e. $\bar{P}_i W_{i;j} = \bar{P}_j W_{j;i}$; the equilibrium probability of one configuration is then proportional to its Boltzman's factor: $\bar{P}_i^{\text{therm}} \propto \exp -\frac{E_i}{kT}$. In the driven system we consider, energy is continuously injected into the system by the collisions of the particles with the atoms, and absorbed by the thermostat. Such a energy flow may sustain *probability fluxes*, the divergence of which is zero for stationary systems. Four strategies are being employed with some success:

- brute force kinetic Monte Carlo simulation of a system governed by the same transition probabilities than the ME;
- effective Hamiltonian ansatz;
- stochastic potentials deduced from a ME for macro variables: application to order–disorder transitions;
- mean field approximation for the kinetics of concentration fields.

3.2.1. Kinetic Monte Carlo modeling

For a description of the method, see [15]. The key step is to give $W_{i,j}^{\text{therm}}$ a physically founded expression. For diffusion controlled recovery processes, $W_{i,j}^{\text{therm}}$ is given by the set of exchange frequencies of atoms with nearest neighbor point defects. The activation barrier for the latter should be written with care, as a function of the occupation of the neighboring sites. One expression commonly used in the kinetic Monte Carlo community, which is blindly extrapolated from the so-called kinetic Ising model, is often misleading [4]. As for $W_{i,j}^{\text{bal}}$, it may be modeled either as randomly distributed (in space and time) flips of nearest neighbor pairs, or as correlated replacements of several atoms at once, as is the case in a displacement cascade. One example of such a simulation will be discussed later.

3.2.2. Effective Hamiltonian ansatz

It consists in giving the solution of Eq. (3), the form $\bar{P}_i \propto \exp-(E_i + \delta H_i^{\text{eff}})/(kT)$; at thermal equilibrium, $\delta H_i^{\text{eff}} = 0$. Giving δH_i^{eff} the same form as the configuration Hamiltonian E_i (e.g. sum of pair interactions) allows one to solve Eq. (3) to a controlled level of approximation. The technique was introduced in the present field by Vaks et al. [16], and has been since used by several groups [17,13]. An empirical justification of the above technique can be given as follows: run a kinetic Monte Carlo simulations, with a simple configurational Hamiltonian,

$$E_i = \frac{1}{2} \sum_{\alpha, \beta; p, q} \eta_p^\alpha \varepsilon_{pq}^{\alpha\beta} \eta_q^\beta$$

($\eta_p^\alpha = 1$ if site p is occupied by a type α particle, and $= 0$ else; index i is omitted); $\varepsilon_{pq}^{\alpha\beta}$ is the contribution to the energy of a pair of atoms with α on site p and β on site q . The kinetics is given by thermally activated flips of nearest neighbor pairs together with, in parallel, ballistic flips of pairs (within some range). A stationary short-range order results, which can be characterized by the intensity of the spherically averaged Fourier components of the occupation number η_p^α . An inverse Monte Carlo technique is then used in order to find what the effective $\varepsilon_{pq}^{\alpha\beta}$'s should be to generate, at thermal equilibrium, the stationary short range order found with the two flip mechanisms acting in parallel. While effective pair interactions can be generated using this procedure [16], it is not yet known whether safe predictions could then be made using models that would include these effective pair interactions but ignore three-body and other multiple body effective interactions.

3.2.3. Stochastic potentials: A2 \Leftrightarrow B2 order–disorder transition

Defining the state of the system at a macroscopic scale by a macro-variable, a master equation can be written for the macro-variable [18,19]. The situation is very simple when the macro-variable is a scalar. Such is the case for the A2 \Leftrightarrow B2 transition on the body centred lattice (e.g. in Fe–Al); in the disordered state (A2), the two simple cubic sublattices, which constitute the BCC lattice, are equally populated; in the fully ordered state, all Fe atoms occupy one of the sublattices, all Al atoms occupy the other one. The degree of order can be defined by the number, n , of Al atoms, which are located on the proper sublattice: $0 \leq n \leq \Omega$, the total number of sites on one sublattice. The transition probabilities are now, $W_{n;n+k}$, i.e. the probability that one sublattice hosting n Al atoms, receives k more such atoms per unit time. The divergence of the probability flux is zero under steady state conditions, but this does not imply necessarily that the flux itself cancels out. In the particular case where $k_{\text{max}} = 1$, however, the stationary probability flux has to be zero at the boundaries $n = 0$ and $n = \Omega$, and this implies that this probability flux is zero everywhere: $\bar{P}_n W_{n;n+k} = \bar{P}_{n+k} W_{n+k;n}$. We get:

$$\frac{\bar{P}_n}{\bar{P}_{n-1}} = \frac{W_{n-1;n}}{W_{n;n-1}} \Leftrightarrow \frac{\bar{P}_n}{\bar{P}_{n_0}} = \prod_{n_0+1}^n \frac{W_{v-1;v}}{W_{v;v-1}} = \exp 2\Omega [\psi(n) - \psi(n_0)]$$

$$\bar{P}_n = \exp 2\Omega [\psi(n) - \hat{\psi}] \quad \text{with} \quad 2\Omega \hat{\psi} = \text{Ln} \left(\sum_0^\Omega \exp 2\Omega \psi(n) \right) \quad (4)$$

$\Psi(n)$ is a stochastic potential, much in the same way as a free energy per lattice site, for a thermodynamic system. Stable stationary macro-states maximize Ψ ; the higher the maximum value, the more stable the macro-state. Detailed calculations show that when the irradiation intensity is set to zero ($W_{n;n\pm 1}^{\text{bal}} = 0$), $\Psi(n)$ reduces to $-F(n)/kT$, with $F(n)$ the free energy of the macro-state as computed in the corresponding mean field approximation.

Similar calculations, slightly more sophisticated, can be performed when more than one atom at a time can change lattice site ($0 < k \leq k_{\text{max}}$), so that the model sheds some light on the effect of the size of replacement cascades. Based on such a formalism, it could be shown that the A2 \Leftrightarrow B2 transition (which is of second type for nearest neighbor interactions) becomes of first type beyond some threshold irradiation intensity; the congruent transformation temperature in the stoichiometric compound could be computed (in the simplest mean field approximation), as well as the phase boundaries in the composition, temperature, irradiation intensity diagram. The shift of the transition line as a function of the size of the cascades (k_{max}) is also computed.

Typical results are summarized in Fig. 5.

Similar effects of the size of a cascade have been found for other order–disorder transitions (e.g. in Ni₄Mo) and sometimes confirmed by experiment [20]. Other effects of the size of cascades have been identified, using brute force KMC. In particular, in the FCC lattice, precipitates with the L1₂ structure dissolve under irradiation following two distinct paths depending on the cascade size: for given displacement rate and temperature, rare large cascades progressively dissolve the precipitates, which retain the L1₂ structure, while frequent small cascades first disorder the L1₂ structure and then dissolve the precipitates. Such effects have practical implications for precipitate strengthening.

3.3. Diffusion fields under irradiation

As stated, nuclear collisions have three distinct effects on solid-state diffusion:

- replaced atoms are moved in a random direction to a relocation distance which usually is equal to or exceeds the nearest neighbor distance;
- displaced atoms produce Frenkel pairs, i.e. vacancies and interstitials, in excess of the thermal equilibrium concentration, with two consequences:
 - the probability for an atom exchanging with a defect is increased (because defects are more numerous);
 - defect fluxes to defect sinks are sustained, because more defects reach a sink than leave the latter sink. As is well known, fluxes are kinetically coupled: a flux of defects drives solute fluxes, in the same or in the opposite direction. Sustained fluxes will induce solute redistribution at defect sinks (or at recombination centers).

3.3.1. Competition between ballistic and thermally activated diffusion

For simplicity, we restrict this discussion to the evolution of the composition field, and we focus on the competition between the forced mixing resulting from atomic replacements and thermal diffusion in a binary alloy system that would undergo phase separation at thermodynamic equilibrium. We show, in particular, that the outcome of this competition depends not only on the relative rates of forced mixing over thermal diffusion, but also on the range of relocation distance. We restrict ourselves to cases where thermal diffusion and atomic replacements are isotropic, in which case we can use a one-dimensional kinetic mean field model to follow the evolution of the composition profile, $c(x)$, during irradiation [8]. This evolution is the sum of a thermally activated term, for which the classical Cahn diffusion model can be used, and a ballistic term:

$$\frac{dc(x)}{dt} = M' \nabla^2 \frac{\delta F}{\delta c} - \Gamma_b \left\{ c(x) - \int w_R(x-x') c(x') dx' \right\} \quad (5)$$

where M' is the thermal atomic mobility, here accelerated by the irradiation, F the free energy of the system, Γ_b the jump frequency of the atomic relocations forced by the nuclear collisions, and w_R is the normalized distribution of relocation distances, characterized by a decay length R [21].

The new length scale R introduced by the irradiation plays a critical role in the evolution of $c(x)$. To illustrate this point, we perform a linear stability analysis in Fourier space. This procedure parallels the classical analysis of spinodal decomposition in the linear regime. The amplification factor $\omega(q)$ of the Fourier coefficient for the wavevector q is given by:

$$\omega(q)/M = -(\partial^2 f / \partial c^2) q^2 - 2\kappa q^4 - \gamma R^2 q^2 / (1 + R^2 q^2) \quad (6)$$

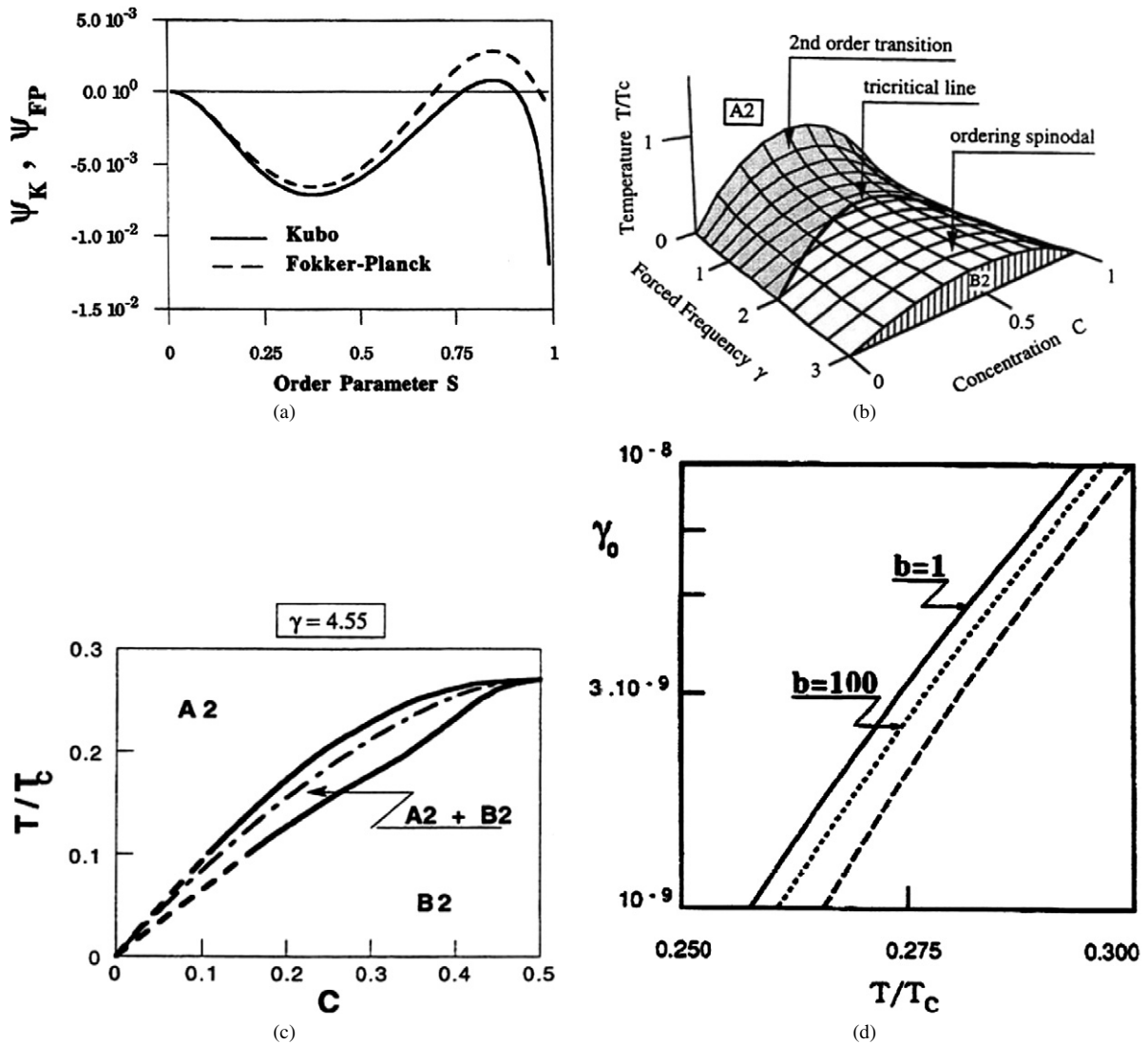


Fig. 5. The dynamical equilibrium of phases A2 and B2 under irradiation: (a) stochastic potential computed in the simplest mean field approximation (point approximation with nearest neighbor interactions); (b) instability limit of the A2 phase in the composition, temperature, irradiation intensity space (the ‘forcing intensity γ' ’ is the ratio of the ballistic to the thermally activated-flip frequency of nearest neighbor pairs); (c) iso-forcing cut of the diagram, beyond the tricritical line: a temperature – composition field is revealed where A2 and B2 domains coexist; (d) when increasing the size of the cascade, as modeled by $b = k_{max}$, the temperature of the congruent transformation is increased keeping the irradiation intensity the same [19].

Fig. 5. Diagramme d’équilibre dynamique des phases A2 et B2 sous irradiation : (a) potentiel stochastique calculé dans l’approximation de champ moyen de point avec des interactions de premiers voisins ; (b) limite d’instabilité de la phase A2 dans le domaine composition–température–intensité d’irradiation (« l’intensité d’irradiation γ » est le rapport de la fréquence d’échanges de paires de premiers voisins par saut balistiques à celle d’échanges par sauts thermiquement activés) ; coupe iso-forçage du diagramme au-delà de la ligne tricritique : il existe un domaine température–composition où les phases A2 et B2 coexistent ; en accroissant la taille des cascades, modélisé par $b = k_{max}$, la température de transformation congruente augmente pour une intensité donnée d’irradiation (d’après [18]).

where $f(c)$ is the free energy density of a homogeneous alloy of composition c , κ the gradient energy, and $\gamma = \Gamma_b/M'$ is a reduced ballistic jump frequency. We restrict the following discussion to compositions and temperatures such that, in the absence of irradiation, spinodal decomposition takes place, i.e., $\partial^2 f/\partial c^2 < 0$.

Let us first consider the limiting case when R is small compared to interplanar lattice spacing. In this case, the third term in Eq. (6) reduces to $(-\gamma R^2 q^2)$. It can then be absorbed in the first term of the right-hand side of Eq. (6), as the

two terms have the same q -dependence. This can be interpreted as introducing an effective free energy that controls the stability of the alloy under irradiation. Using a regular solution model for $f(c)$, one shows that this effective free energy is in fact nothing more than the equilibrium free energy of the alloy evaluated at an effective temperature $T_{\text{eff}} = T(1 + \Gamma_b/\Gamma'_{\text{th}})$. In the small R limit, we thus recover the effective temperature criterion introduced by G. Martin in 1984 [22]. This criterion predicts that, depending upon the irradiation flux and the irradiation temperature, pre-existing precipitates should either dissolve, or they should continuously coarsen with time.

We turn to the case where R is larger than the interplanar spacing. It now becomes possible to find irradiation intensities γ such that the ballistic term in Eq. (6) is greater than $|\partial^2 f/\partial c^2|$ at small q , but smaller than $|\partial^2 f/\partial c^2|$ at large q . In such cases, the amplification factor is first negative for small q values, but it becomes positive when q exceeds some critical value, q_{min} , while for larger q , the amplification factor is negative again. Therefore, decomposition is still expected to take place, but only for wavevectors larger than q_{min} , i.e., for wavelengths smaller than $2\pi/q_{\text{min}}$. We thus anticipate that coarsening may saturate, since at large length scales, the alloy remains stable with respect to decomposition. In other terms, the composition field will self-organize into patterns with a characteristic length scales $2\pi/q_{\text{min}}$. In this case, it is no longer possible to an effective temperature for alloy stability under irradiation, but one can then rely on the effective Hamiltonian approach introduced in Section 3.2.2 [10].

We have verified these predictions using a variational analysis of Eq. (5) [8], which includes non-linear effects, and we used this analysis to construct the dynamical phase diagram displayed in Fig. 2(b). As seen on this diagram, when the characteristic length for the forced relocation is smaller than a critical value, R_c , the system never develops patterns at steady state. Above R_c , patterning takes place when the irradiation conditions are chosen so as to result in an appropriate γ value. The characteristic length of the most stable pattern can be varied continuously by varying γ , but the upper limit for the pattern size is $2\pi R$.

With this formalism in mind, we can discuss the problem of the stability of gas bubbles introduced in Section 3.1. Since nuclear collisions simply add a ballistic contribution to the random walk of the various species, the rate of decay due to ballistic events is simply written:

$$\partial n^{\text{irrad}}/\partial t \propto -4\pi R D^{\text{bal}}(c_p - c);$$

the ballistic contribution has the same dependence in R as the thermal contribution; no stationary radius is to be expected, from this simple model. The stabilization of the bubble size, if it is observed, is a manifestation of the patterning process discussed above.

In the case of chemical ordering, where the relevant field required to describe the microstructure is a non-conserved order parameter, patterning of the field of chemical order can also be triggered by irradiation, but this time when the size of the disordered zone exceeds a given threshold value [23–25].

3.3.2. Defect fluxes and precipitate stability

Forgetting about ballistic effects, the kinetics of concentration fields under irradiation is described by the following set of partial derivative equations:

$$\partial_t c_d = K_d - K_{iv} c_i c_v - K_{df} c_d - \nabla \cdot J_d$$

for the defects d (interstitials i or vacancies v). K_d is the defect production rate, K_{iv} the rate constant for the recombination of Frenkel pairs, K_{df} the rate constant for defect elimination on a homogenized population of fixed sinks, J_d the defect flux at a scale larger than the latter homogenization length.

$$\partial_t c_s = -\nabla \cdot J_s \quad \text{for the solutes } (s_1, s_2, s, \dots)$$

Each flux can be written:

$$J_\alpha = -\sum_{\beta} D_{\alpha\beta}^{\text{therm}} \cdot \nabla c_\beta; \quad \alpha, \beta = i, v, s_1, s_2, s, \dots$$

where the diffusion matrix is given by:

$$D_{\alpha\beta}^{\text{therm}} = \sum_{\gamma} L'_{\alpha\gamma} \cdot f_{\gamma\beta}, \quad \text{with } f_{\alpha\beta} = \frac{\partial(\mu_\alpha - \mu_{\text{Solvent}})}{\partial c_\beta}$$

The L matrix (definite, positive, symmetric) reflects the kinetic couplings among fluxes: indeed, whenever the various solutes exchange with the defects with distinct frequencies, a flux of defect triggers solute redistribution. The $f_{\alpha\beta}$

matrix (susceptibility matrix) reflects the thermodynamics couplings among fluxes: indeed, because of solute–solute interactions, a flux of species β drives a flux of any other species (see [26]). Notice the superscript L' which is here to recall that atomic mobility is enhanced by the defect supersaturation ($L' > L$).

The above equations reveal the two distinct effects of irradiation induced defect supersaturation:

- accelerating thermodynamical evolutions, because of the enhanced atomic mobility ($L' > L$);
- biasing the evolution: indeed, because the defect supersaturation sustained by irradiation is large, ∇c_d under irradiation may strongly differ from its equilibrium value. As a result, solute redistribution may build up at the scale of the dominant defect sink population, or at some intrinsic scale dictated by the recombination length, whenever defects mainly annihilate by mutual recombination. One example is the formation of Guinier Preston zones in dilute Al(Zn) solid solutions, under intense 1 MeV electron irradiation, at temperature well above the solvus (see Fig. 1; for a summary, cf. [5]).

Non-equilibrium, irradiation induced segregations at grain boundaries, or at dislocation lines are very common, with important practical implications.

4. Conclusions

From this brief survey, one should keep in mind that for a given material, the structure that resists irradiation may not be unique. In all events, the structure that develops depends on three types of irradiation parameters:

- (i) the cascade features (e.g. distribution of relocation lengths, number of relocation events per cascade, ...),
- (ii) the frequency at which cascades do occur,
- (iii) the cumulated irradiation dose.

In practice, there is no generic name for (i); (ii) is named the dose rate or irradiation intensity, or flux, and (iii) is named the dose, or the fluence. As we have seen, when dealing with stationary states, the cumulated dose is of weak importance, while the cascade features play an important role. By analogy with medicine, where a ‘dose’ is the unit of drug intake, one may think of the cascade as an elementary irradiation dose; the intensity of an irradiation, is then defined by the rate of delivery of doses, i.e. the dose rate, and the total number of doses delivered is the fluence. We believe such a nomenclature would clarify several debates, such as the ‘effect of small doses’.

Acknowledgements

One of us (P.B.) acknowledges support from U.S. Department of Energy, Division of Materials Sciences under Award No. DEFG02-05ER46217, through the Frederick Seitz Materials Research Laboratory at the University of Illinois at Urbana-Champaign.

References

- [1] Y. Adda, M. Beyeler, G. Brebec, *Thin Solid Films* 25 (1975) 107.
- [2] J. Pauleve, A. Chamberod, K. Krebs, A. Bourret, *J. Appl. Phys.* 39 (1968) 989.
- [3] (a) A. Barbu, G. Martin, *Scripta Metall.* 11 (1977) 771;
(b) R. Cauvin, G. Martin, *Phys. Rev. B* 23 (1981) 3333.
- [4] G. Martin, P. Bellon, *Solid State Phys.* 50 (1997) 189.
- [5] P. Bellon, G. Martin, *Kinetics in nonequilibrium alloys*, in: W. Pfeiler (Ed.), *Alloy Physics*, Wiley-VCH, Weinheim, 2007, p. 423.
- [6] M. Zaiser, F. Banhart, *Phys. Rev. Lett.* 79 (1997) 3680.
- [7] M. Zaiser, Y. Lyutovich, F. Banhart, *Phys. Rev. B* 62 (2000) 3058.
- [8] R.A. Enrique, P. Bellon, *Phys. Rev. Lett.* 84 (2000) 2885.
- [9] R.A. Enrique, P. Bellon, *Phys. Rev. B* 63 (2001) 134111.
- [10] R.A. Enrique, P. Bellon, *Phys. Rev. B* 70 (2004) 224106.
- [11] R.S. Nelson, J.A. Hudson, D.J. Mazey, *J. Nucl. Mater.* 44 (1972) 318.
- [12] P. Gaspard, *Physica A* 369 (2006) 201–246.
- [13] C. Tsallis, E. Brigatti, *Continuum Mech. Thermodyn.* 16 (2004) 223.

- [14] F. Soisson, P. Dubuisson, P. Bellon, G. Martin, in: W.C. Johnson (Ed.), *Solid–Solid Phase Transformations*, TMS, 1994, p. 981.
- [15] T. Abinandanan, F. Haider, G. Martin, *Acta Mater.* 46 (1998) 4243.
- [16] V.G. Vaks, V.V. Kamyshenko, *Phys. Lett. A* 177 (1993) 269.
- [17] R. Enrique, P. Bellon, *Phys. Rev. B* 60 (1999) 14649.
- [18] R. Kubo, K. Matsuo, K. Kitahara, *J. Stat. Phys.* 9 (1973) 51.
- [19] P. Bellon, G. Martin, *Phys. Rev. B* 39 (1989) 2403.
- [20] P. Bellon, P.R. Okamoto, G. Schumacher, *J. Nucl. Mater.* 205 (1993) 438.
- [21] R.A. Enrique, K. Nordlund, R.S. Averback, P. Bellon, *J. Appl. Phys.* 93 (2003) 2917.
- [22] G. Martin, *Phys. Rev. B* 30 (1984) 1424–1436.
- [23] Jia Ye, P. Bellon, *Phys. Rev. B* 70 (2004) 094104.
- [24] Jia Ye, P. Bellon, *Phys. Rev. B* 70 (2004) 094105.
- [25] Jia Ye, P. Bellon, *Phys. Rev. B* 73 (2006) 224121.
- [26] A.R. Allnatt, A.B. Lidiard, *Atomic Transport in Solids*, Cambridge University Press, 1993.